Bioactive Materials 46 (2025) 569–581

Contents lists available at ScienceDirect

Bioactive Materials

journal homepage: www.keaipublishing.com/en/journals/bioactive-materials

Synergistic restoration of spinal cord injury through hyaluronic acid conjugated hydrogel-polydopamine nanoparticles combined with human mesenchymal stem cell transplantation

Yanbing Kao [a,c,1], Wei Song [a,c,1], Renjie Zhang [b,c,1], Guangjin Gu [a,c], Heping Qiu [c], Wenyuan Shen [b,c], Hanming Zhu [a,c], Yanchun Liu [a,c], Yu Yang [a,c], Haoyun Liu [a,c], Zhihao Zhang [a,c], Xiaohong Kong [a,c,**], Shiqing Feng [a,b,c,*]

[a] Department of Orthopedics, Qilu Hospital of Shandong University, Jinan, Shandong, China
[b] Department of Orthopedics, Second Hospital of Shandong University, Jinan, Shandong, China
[c] Orthopedic Research Center of Shandong University &Advanced Medical Research Institute, Cheeloo College of Medicine, Shandong University, Jinan, Shandong, China

ARTICLE INFO

Keywords:
Spinal cord injury
Polydopamine nanoparticles
Endogenous neural stem progenitor cells
Human mesenchymal stem cells

ABSTRACT

Spinal cord injury (SCI) is a devastating disease with limited treatment options due to the restricted regenerative capacity of the central nervous system. The accumulation of reactive oxygen species (ROS) and inadequate endogenous neural stem progenitor cells (eNSPCs) in the lesion site exacerbates neurologic deficits and impedes motor function recovery. We have developed a temperature-responsive hyaluronic acid conjugated hydrogel-polydopamine nanoparticles (PDA NPs) combined with human mesenchymal stem cell (hMSCs) transplantation, denoted as H-P-M hydrogel. Microglia cells treated with PDA NPs have been shown to reduce intracellular ROS levels by 65 % and suppress the expression of inflammatory cytokines such as IL-1β (decreased by 35 %) and IL-6 (decreased by 23 %), thus mitigating the microglia's inflammatory response. Additionally, our results have demonstrated that the H-P-M hydrogel combined with hMSCs transplantation can recruit eNSPCs to the injury site as evidenced by utilizing Nestin lineage tracer mice. The RNA-seq has unveiled the potential of the H-P-M hydrogel to facilitate eNSPCs neuronal differentiation through the MAPK pathway. Furthermore, these differentiated neurons are integrated into local neural circuits. Together, it suggests that the H-P-M hydrogel synergistically improves the SCI niche. It serves as catalysts inducing 5-HT axon regeneration and improving BMS score after SCI through the modulation of the ROS milieu and the promotion of neuronal differentiation from eNSPCs, thereby presenting a promising strategy for SCI repair.

1. Introduction

Spinal cord injury (SCI) is severe central nervous system (CNS) trauma, resulting in enduring motor, sensory and/or autonomic dysfunction [1]. Given the restricted regenerative capacity of CNS and the complex pathology, effective treatment strategies for SCI are currently lacking [2,3]. Complications such as paralysis and neuropathic pain affect the quality of life for SCI patients and cause a significant burden upon society.

Over the past decade, cell transplantation using hydrogel scaffold has emerged as a promising strategy for SCI repair [4]. Stem cell transplantation, particularly with mesenchymal stem cells (MSCs), offers the potential to secret neurotrophic factors and builds a favorable microenvironment for endogenous neural stem progenitor cells (eNSPCs) neuronal differentiation. Meanwhile, hydrogel scaffolds provide essential mechanical supports for cell growth and bridging the injury site [5]. Hyaluronic acid (HA) represents a natural material well-suited for hydrogel preparation due to its favorable compatibility [6]. HA hydrogels can be engineered to possess highly porous structures and viscoelasticity properties closely resembling those of natural CNS tissue.

Peer review under responsibility of KeAi Communications Co., Ltd.
* Corresponding author. Department of Orthopedics, Qilu Hospital of Shandong University, Jinan, Shandong, China.
** Corresponding author. Department of Orthopedics, Qilu Hospital of Shandong University, Jinan, Shandong, China.
E-mail addresses: kongxh@sdu.edu.cn (X. Kong), shiqingfeng@sdu.edu.cn (S. Feng).
[1] These authors contribute equally to the work.

https://doi.org/10.1016/j.bioactmat.2024.09.027
Received 31 May 2024; Received in revised form 19 September 2024; Accepted 19 September 2024

Moreover, HA is amendable to various modifications aimed at customizing the characteristics of resulting materials [7,8]. In this study, the dopamine modification has conferred creative adhesive properties upon the HA hydrogel, facilitating its adhesion to spinal cord tissue.

In addition to chemical modification, the incorporation of nanoparticles can enhance the therapeutic potential of hydrogels significantly. Polydopamine nanoparticles (PDA NPs) are generated through the self-polymerization of dopamine with multi-functionality, attracting considerable attention in many biomedical applications [9]. PDA is derived from adhesive proteins secreted by mussels, characterized by meritorious biocompatibility, biodegradability and other unique biochemical properties, including ultraviolet (UV) absorption, photothermal transformation, free radical scavenging and drug delivery [10,11]. The capacity of PDA to scavenge ROS by its phenolic hydroxyl groups, suggests a novel therapeutic avenue for SCI; while recent studies have highlighted the promising anti-inflammatory properties of PDA either *in vitro* or *in vivo*, the applications of PDA NP for SCI repair are not available yet [10,12].

In this study, we constructed HA conjugated PDA NP-hydrogel during the gelation between HA chains where dispersed PDA NPs within the hydrogel (Fig. 1). The resulting dopamine-modified hydrogel stimulates the adhesion and growth of stem cells with being bridging of nerve tissue. Moreover, the PDA NPs alleviate the oxidative milieu and ameliorate inflammatory response. Subsequent evaluation in the spinal cord transection model demonstrated that H-P-M hydrogel reducing inflammation and promoting eNSPC neuronal differentiation, consequently improving motor function after SCI.

2. Materials and methods

2.1. Synthesis of HA-DA polymer

Briefly, 500 mg HA (Yuanye, Shanghai, China) was dissolved in 100 ml deionized water. Then, 150 mg N-(3-dimethylaminopropyl)-N-ethylcarbodiimide (Sigma-Aldrich, MO, USA) and 200 mg dopamine hydrochloride (Sigma-Aldrich, MO, USA) were added to the HA solution at pH 5 adjusted by hydrochloric acid (Sigma-Aldrich, MO, USA). Subsequently, the reaction was performed continuously under nitrogen protection for 24 h. Unreacted chemicals and byproducts were removed by dialysis for 48 h in deionized water at pH 5. Finally, the resulted product was lyophilized and stored at 4 °C for further use.

2.2. Synthesis of PDA NPs

Briefly, 180 mg dopamine hydrochloride (Sigma-Aldrich, MO, USA) was dissolved in 90 ml deionized water. Then, 0.38 ml of 1 M NaOH solution was added to above solution. After self-polymerization for 2 h, PDA NPs were obtained by centrifugation.

2.3. Hydrogel preparation

Briefly, 15 mg HA-DA powder was dissolved in 750 μl PBS solution with the help of ultrasonication. Then, the various concentrations of PDA NPs (0, 10, 20 and 50 μg/ml) and/or 1×10^6 human umbilical cord mesenchymal stem cells (hUC-MSCs) were added to above solution. The gelation reaction proceeded with 50 μl of $NaIO_4$ (0.84 mg/ml) at 37 °C.

2.4. Characterization of hydrogel properties

Fourier transform infrared (FTIR) spectroscopy: After drying, the HA powder and HA-DA powder are mixed with KBr crystal powder and ground separately. The two samples are then pressed into pellets. The FTIR is used to analyze the infrared spectra of the two samples in the wavenumber range of 500 cm^{-1} to 4000 cm^{-1}.

Scanning electron microscope (SEM): The hydrogel was freeze-dried in a freeze dryer for 24 h. Then, the freeze-dried sample was broken in liquid nitrogen to obtain a cross-section. Subsequently, it was gold-coated for observation of the hydrogel's internal microstructure using scanning electron microscope (SEM).

Nuclear magnetic resonance spectroscopy: The experiment was performed on a Bruker Avance Neo 600 MHz spectrometer equipped with a QCI 5 mm cold probe and a SampleJet automatic sample changer. 15 mg HA or HA-DA powder were dissolved in 750 μl of D_2O and placed in an NMR tube. The NMR hydrogen spectra of the two samples were detected at 300 Hz.

Rheological test: The rheological properties were measured with the

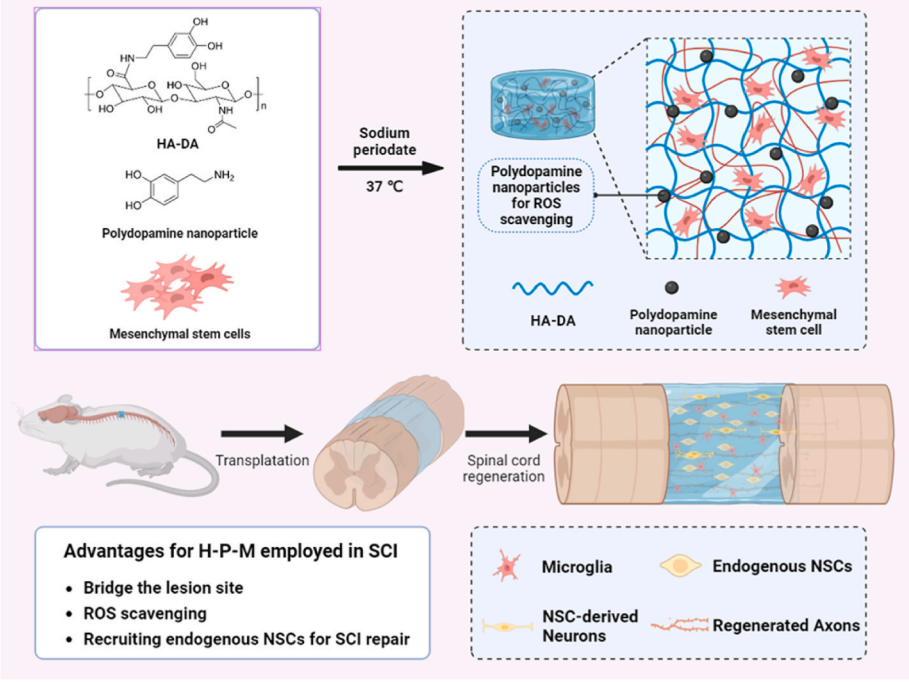

Fig. 1. Schematic diagram of the preparation and use of the multifunctional hydrogel scaffold for SCI repair.

Rheometer (Haake Mars60, Germany). Hydrogels were placed onto the parallel plate and preheated to 37 °C to solidify it, then lowered the upper plate to l mm gap for detection. For oscillatory time sweep experiments, the storage and loss moduli were measured at 10 Hz and 1 % strain.

2.5. Cell viability assay

Cell viability was assessed using the CCK8 kit (Hanbio, Shanghai, China). The hUC-MSCs were seeded in 24-well culture plates at a density of 5×10^4 cells per well. After incubation with different concentrations of PDA NPs (0, 10, 20 and 50 μg/mL) for 1, 3 and 7 days, 50 μl of CCK8 was added to each well. After incubation at 37 °C for 2 h in an incubator with 5 % CO_2, the readouts at 450 nm of the plate reader indicated the cell viability.

2.6. ROS assay

The BV2 cells were seeded in 24-well culture plates at a density of 2×10^5 cells. We added 500 μl DMEM containing 10 μM DCFH-DA (Beyotime Biotechnology, Shanghai, China) to each well, and then incubated for 20 min. Next, we removed the culture medium and wash three times using PBS. Finally, the cellular ROS level (DCFH-DA fluorescence intensity) was detected by a microplate reader (Thermo Scientific, MA, USA).

2.7. 3D culture of hUC-MSCs in vitro

To assess the protective effect of PDA NP-decorated hydrogel or blank hydrogel for hUC-MSCs against ROS, the hUC-MSCs were encapsulated in the 3D hydrogel. The size of 3D hydrogels is 8.4 mm × 4.2 mm × 5 mm (length × width × height). Then, 100 μM H_2O_2 was added to culture medium to create ROS microenvironment. After the peroxidative culture for 24 h, the cell survival rate of different group was assessed using a Live/Dead staining kit (Beyotime Biotechnology, Shanghai, China) following the manufacturer's instructions. 3D fluorescence imaging was performed using a laser microscope (Zeiss LSM 900, Germany).

2.8. Reverse transcription and quantitative PCR

Total RNA was extracted using TRIzol following the manufacturer's instructions (15596026, Invitrogen, Waltham, MA, USA). CDNA was synthesized with a cDNA reverse transcription kit (KR116-02, Tiangen, China) from 2 μg total RNA. The qPCR was performed using SYBR Green (AQ601, TransGen Biotech, Beijing, China) and the LC96 real-time PCR detection system (Roche, Mannheim, Germany) according to the provided instructions.

2.9. Western blotting

The Western blot was performed following previously published protocols [13]. The primary antibodies including anti-GFAP (1:1000, CST, 3670s), anti-Tuj1(1:2000, abcam, ab215037), anti-GAPDH (1:10000, proteintech, 10494-1-AP), anti-p-ERK (1:1000, diagbio, db13437), anti-p-JNK (1:1000, diagbio, db3253), anti-Actin (1:1000, proteintech, 66009-1), anti-JNK (1:1000, diagbio, db14225), anti-ERK (1:2000, diagbio, db11649). The secondary antibodies used were anti-mouse HRP (1:10000, proteintech, SA00001-1), anti-rabbit HRP (1:10000, proteintech, SA00001-2).

2.10. Neuronal differentiation assay

To assess the effect of hMSCs on NSPCs neuronal differentiation, we performed a co-culture of hMSCs and NSPCs using transwell at a ratio of 1:1. After 7 days of cultivation, the expression of neuronal and astrocytic markers Tuj1, Map2 and GFAP was detected using immunofluorescence (IF) assay and also quantitated using RT-qPCR and Western blot.

2.11. RNA-seq

TRIzol reagent (15596026, Invitrogen, USA) was used to extract total RNA from spinal cord tissue, following the manufacturer's instructions. Novogene (Beijing, China) conducted RNA-sequencing for the obtained RNA samples. The NEBNext Ultra™ Directional RNA Library Prep Kit for Illumina was used to generate sequencing libraries. An index of the reference genome was built using Hisat2 (v2.0.5) and paired-end clean reads were aligned to the reference genome using Hisat2 (v2.0.5). Following the alignment, feature counts (v1.5.0-p3) were used to analyze differential gene expression, utilizing the BAM files obtained from each alignment.

2.12. Contusion SCI model

Fifty-four female C57BL/6 mice (22–25 g) of 8–10 weeks of age were obtained from Vital River Laboratory Animal Technology Co., Ltd. These mice were randomly divided into six groups (Sham, SCI, HA hydrogel, HA hydrogel with hMSCs, HA hydrogel with PDA NPs, HA hydrogel with PDA NPs and hMSCs, each group n = 9). On the day before modeling, all mice were administered cyclosporine A (HY-B0579, MCE, USA) via intraperitoneal injection at a dosage of 10 mg/kg/day. The transection SCI model was established on the next day following previously published protocols [5,14]. The spinal cord was transected to make a 2 mm gap. Next, a 5 μl hydrogel solution with or w/o hMSCs (5×10^4 cells/μl) and PDA NPs (20 μg/ml) was injected into the tissue cavity at the injury site immediately after injury. After 5 min, the muscle and skin were sutured. Cell transplantation completed in one procedure, no further transplantations are required. Manual bladder emptying was performed twice daily. All mice received a cefuroxime injection once a day for 7 days after surgery. All mice received intraperitoneal injection of cyclosporine A (HY-B0579, MCE, USA) at a dosage of 10 mg/kg, administered daily until the end of the experiment.

2.13. Perfusion and sectioning

Mice were anesthetized with isoflurane, and the heart was exposed after opening the chest cavity. Pre-cooled PBS was then perfused through the heart until no blood was observed flowing out and the liver color paled. Subsequently, pre-cooled 4 % paraformaldehyde was transcardiac perfused. The bilateral lamina was carefully removed using spring scissors to fully expose the spinal cord. The spinal cord was collected, and then fixed in 4 % paraformaldehyde for 24 h. To prepare the tissue for further analysis, a concentration gradient sucrose solution was used for dehydration. Subsequently, the dehydrated spinal cords were embedded in OCT mounting media and sectioned at a thickness of 8 μm using a cryotome (Leica, CM3050S, Germany).

2.14. Hematoxylin and eosin (HE) staining

The method of HE was based on the previous study [15]. Briefly, the embedded heart, liver, spleen, lung, kidney and spinal cord tissue were sectioned into 8 μm thick slices using microtome. The sections were then dewaxed and rehydrated with gradient xylene/alcohol and PBS. Hematoxylin and eosin-stained were performed on the tissue for 10 min and followed by eosin staining for 20 s. Finally, the tissue was sealed with neutral resin and directly observed under the microscope NanoZoomer S60 (Hamamatsu, Japan).

2.15. IF assay

The IF assay was performed following previously published protocols [16].The primary antibodies used were rabbit anti-Tuj1 (1:500, abcam,

ab215037), mouse anti-GFAP (1:500, CST, 3670S), rabbit anti-5-HT (1:100, abcam, ab271031), rabbit anti-Syn1 (1:1000, abcam, ab32127), rabbit anti-ARG1 (1:100, abcam, ab233548), mouse anti-Iba1 (1:200, abcam, ab283319), mouse anti-iNOS (1:1000, abcam, ab210823). The secondary antibodies used were 555-Goat Anti-Rabbit (1:200, abcam, ab150082), 488-Goat Anti-mouse (1:200, abcam, ab150117), 488-Goat Anti-rabbit (1:200, abcam, ab150081), 647-Goat Anti-mouse (1:200, abcam, ab150115).

2.16. Basso mouse scale (BMS)

To assess hindlimb locomotor behavior recovery in mice, BMS scores were conducted at various time points: before SCI, and then weekly for 8 weeks, following the Basso Mouse Scale guidelines. Before the tests, mice were acclimated to the round open field environment with a diameter of 1 m. Transparent glass panels surrounded the field, enabling observers to evaluate hindlimb locomotor behavior. Two blinded investigators carried out the experiments, randomly testing and scoring mice from different experimental groups. Each mouse was individually placed in the open field and observed for 4 min. BMS scores ranged from 0 to 9, with each score representing a distinct degree of hindlimb locomotor behavior.

2.17. Catwalk gait analysis

The CatWalk XT system (Noldus, Wageningen, Netherlands) was used to assess the recovery of lower limb motor function in mice as previously described [13]. The CatWalk testing was conducted in a dark room, and a traversal of the runway by the mice within 15 s was considered a valid footprint recording. The collected mouse footprint data was analyzed using the CatWalk XT software. The experimenters conducting the tests were blinded to the treatment groups.

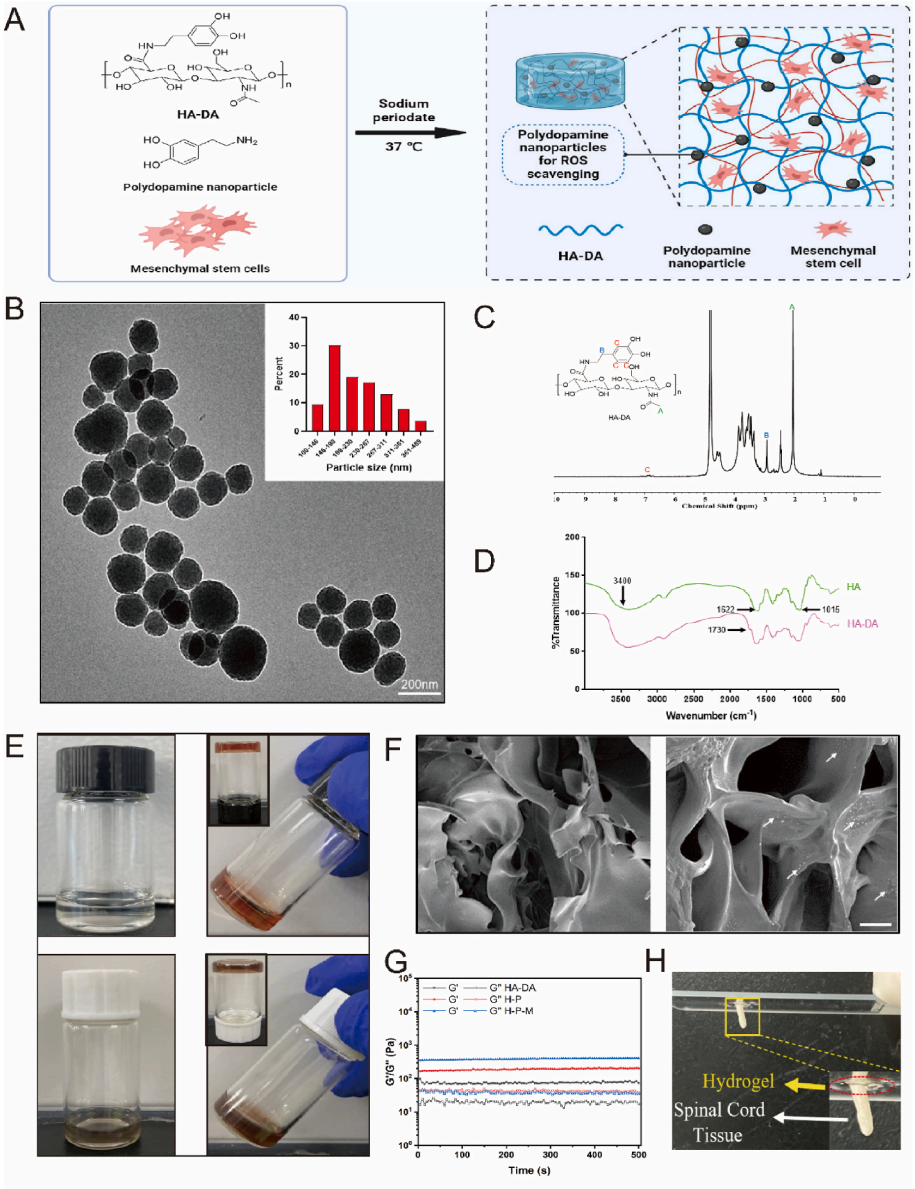

Fig. 2. Preparation and characteristics of PDA NP-decorated hydrogel. (A) Schematic diagram of the gelation of the thermosensitive PDA NP-decorated HA hydrogel. (B) Transmission electron microscopy (TEM) images of PDA NPs. Scale bar: 200 nm. (C) Nuclear magneto-hydrogen spectroscopy (NMR) of HA-DA. (D) The vibration of the FTIR shows the absorption peaks of HA and HA-DA molecules. (E) The gelation of HA-DA loaded with or w/o PDA NPs at 37 °C. (F) Scanning electron microscopy (SEM) images of HA-DA hydrogel (The white arrow indicates the presence of the PDA NPs). Scale bar: 10 μm. (G) Storage modulus (G′) and loss modulus (G″) of HA-DA, H-P and H-P-M hydrogels. (H) The direct view of hydrogel adhesion to spinal cord tissues.

2.18. Electrophysiology examination

The mice were anesthetized with isoflurane. Then, the stimulating electrode and the recording electrode were respectively placed on the cerebral cortex and the sciatic nerve. A single electrical pulse with an intensity of 5 mA was used to record motor evoked potentials (MEPs) using electrophysiological monitoring device (YRKJ-G2008; Zhuhai Yiruikeji Co., Ltd, Guangdong, China).

2.19. Statistical analysis

Statistical analyses were conducted using GraphPad Prism 8 (GraphPad Software, SanDiego, CA, USA). Results were analyzed using one-way ANOVA with the Holm-Sidak test and two-way ANOVA for multiple comparisons or Student's t-test for pairwise comparisons. Statistical significance was defined as a p-value less than 0.05.

3. Results

3.1. Preparation and characterization of PDA NP-decorated hydrogel

The process of fabrication of the PDA NP-dotted hydrogel is depicted in Fig. 2A. Initially, the monomeric dopamine group was introduced onto the HA chains (HA-DA) to enhance adhesion properties; next, the resulting modified products underwent examination through Hydrogen Nuclear Magnetic Resonance (HNMR) (Fig. 2C) and FTIR spectroscopy (Fig. 2D). The HNMR revealed dopamine incorporated well as evidenced by the emergence of the new peak at 6.7 ppm corresponding to the aromatic protons of the dopamine catechol group (Fig. 2C). Similarly, the FTIR spectrum displayed an additional peak at 1730 cm^{-1} in the HA-DA group, indicating the formation of amide bonds during dopamine grafting (Fig. 2D). These findings collectively confirmed that HA-DA contains a benzene ring and methylene structure, validating the grafting of dopamine onto HA.

PDA NPs were synthesized through the oxidative self-polymerization of dopamine. As illustrated in Fig. 2B, PDA NPs exhibited spherical shapes with an average diameter of 230 nm. The PDA NP-decorated hydrogel was prepared by mixing PDA NPs and HA-DA solution and then crosslinking with $NaIO_4$ at 37 °C for 5 min, as depicted in Fig. 2E. The microstructure of the hydrogels was detected using scanning electron microscopy (SEM), displaying the characteristic uniform and interconnected porous network in our synthesized hydrogel, along with the distinct incorporation of PDA NPs, as shown in Fig. 2F. The UV–Vis spectroscopy of HA-DA and HA are presented in Fig. S1A where one specific band at 280 nm appears for the HA-DA group, but it was not observed in the HA group. Based on the absorbance of HA-DA measured at 280 nm, the grafting rate was 12 %. To investigate the hydrogel's mechanical properties and stabilities, the storage modulus (G′) and loss modulus (G'') were assessed using a rheometer. We didn't observe significant temporal correlation between the G′ and G'' within 1–500 s among these groups, indicating stable viscoelastic solid behavior of the hydrogels. Additionally, the G′ of HA-DA hydrogel was significantly increased by the addition of PDA NPs and hMSCs (370.3 ± 1.5 Pa), which was close to the G′ of naïve spinal cord tissue (0.1–16 kPa) (Fig. 2G) [17]. The representative stress-strain curves of H-P-M hydrogel was presented in Fig. S1B. Additionally, the HA-DA hydrogel could closely adhere to the mouse spinal cord tissue and exhibited a significant increase in adhesive force compared with HA hydrogel (1.6 N vs 0.6 N), demonstrating improved adhesion following dopamine modification (Fig. 2H, Fig. S1C). To assess the degradation capacity of the hydrogels, they were immersed in a phosphate-buffered saline (PBS) solution for a designated period. The PDA NP-decorated hydrogel exhibited complete degradation after 14 days (Fig. S2).

3.2. Antioxidant properties and biocompatibility of PDA NP-decorated hydrogel

We assessed the cytotoxicity of the developed hydrogel on hMSCs. CD73, CD90 and CD105 were identified positively as 99.93 %, 99.98 % and 99.98 %, respectively, by flow cytometry analysis in hUC-MSCs where CD34 or CD45 of the hematopoietic stem cell markers were undetectable (Fig. 3A). Subsequently, the osteogenic, adipogenic and chondrogenic differentiation potential of hUC-MSCs were detected. As expected, the hUC-MSCs showed tri-lineage differentiation ability (Fig. 3B–D). To examine the impacts of PDA NPs concentration on hydrogel's biocompatibility, the hUC-MSCs were exposed to increased concentrations of PDA NPs (0, 10, 20 and 50 μg/ml). The cell proliferation assay on day 1, 3 and 7 showed notable cytotoxicity was observed in the 50 μg/ml group (Fig. 3E). Additionally, the viability of hMSCs co-cultured with PDA NPs was detected using Live/Dead staining at 24 h and 48 h, respectively. The results indicated a reduction in viable cells in the 50 μg/ml group, although significant cell death was not observed, suggesting the high concentration of PDA NPs exerts a negative impact on cell proliferation (Fig. 3F).

To further investigate the toxicity of PDA NP-decorated hydrogels loaded with hMSCs (H-P-M hydrogel) *in vivo*, the H-P-M hydrogel was injected into mouse spinal cord tissue. After 8 weeks, the blood tests were performed for liver and kidney function and no significant elevation of indicators of impair function, including blood urea nitrogen (BUN), creatinine (CREA), uric acid (UA), alkaline phosphatase (ALP), aspartate aminotransferase (AST) and alanine aminotransferase (ALT) (Fig. 3H). Additionally, no pathological change observed in heart, kidney, liver, lung and spleen (Fig. 3G), indicating that H-P-M hydrogel did not cause any toxicity to those organs.

To verify the hydrogel's ability to scavenge ROS, BV2 cells treated with LPS were cultured at different concentrations of PDA NPs. After 24 h, the intracellular ROS levels were quantified. The results showed that treatment with 10, 20 and 50 μg/ml of PDA NPs significantly decreased intracellular ROS levels by 52 %, 65 % and 75 % at the 10, 20 and 50 μg/ml of PDA NP compared with the control group (Fig. 4A–B). Furthermore, the mRNA level of inflammatory factors IL-6 and IL-1β in activated BV2 cells reduced by 23 % and 35 %, respectively, following treatment with 20 μg/ml of PDA NPs (Fig. 4C–D). Overall, our results demonstrated PDA NPs effectively scavenge intracellular ROS and reduce the level of proinflammatory factors *in vitro* at the optical concentration of 20 μg/ml. Subsequently, the hUC-MSCs were 3D cultured in hydrogel decorated with 20 μg/ml PDA NPs for 2 days to assess the biocompatibility and biotoxicity. The result showed minimal PI-stained dead cells after 3D culture, suggesting that hUC-MSCs could grow well within H-P-M hydrogel (Fig. S3). Consequently, the hydrogel loaded with 20 μg/ml PDA NPs was selected for subsequent biological experiments. To investigate the protective effect of the hydrogel decorated with 20 μg/ml PDA NPs (H-P hydrogel) to hMSCs in an oxidative microenvironment, the hMSCs cultured in the 3D hydrogels, followed by the addition of 0.1 mM H_2O_2 to the cell culture medium. After 24 h of cultivation, the Live/Dead staining showed a higher cell survival rate in the H-P hydrogel group compared to the blank hydrogel group (64.7 % vs 35.2 %) (Fig. S4). Next, the compatibility of hydrogels with neuron/astrocyte/microglia cells (HT22/C8-D1A/BV2 cells), which are resident cells in the spinal cord, was assessed using the CCK-8 kit and Calcein-PI dye. The H-P-M hydrogel was evaluated for cell viability after 1, 2 and 3 days of co-culture with these cells, and no significant difference in cell survival rate between the control and H-P-M group (Fig. S5).

3.3. The H-P-M hydrogel facilitated the differentiation of NSPCs to neurons in vitro

Next, PDA NP-decorated hydrogels loaded with hMSCs (H-P-M hydrogel) exemplified by the neurosphere formation and positive Nestin and SOX2 in the neurospheres (Fig. S6). After 7 days, NSPCs

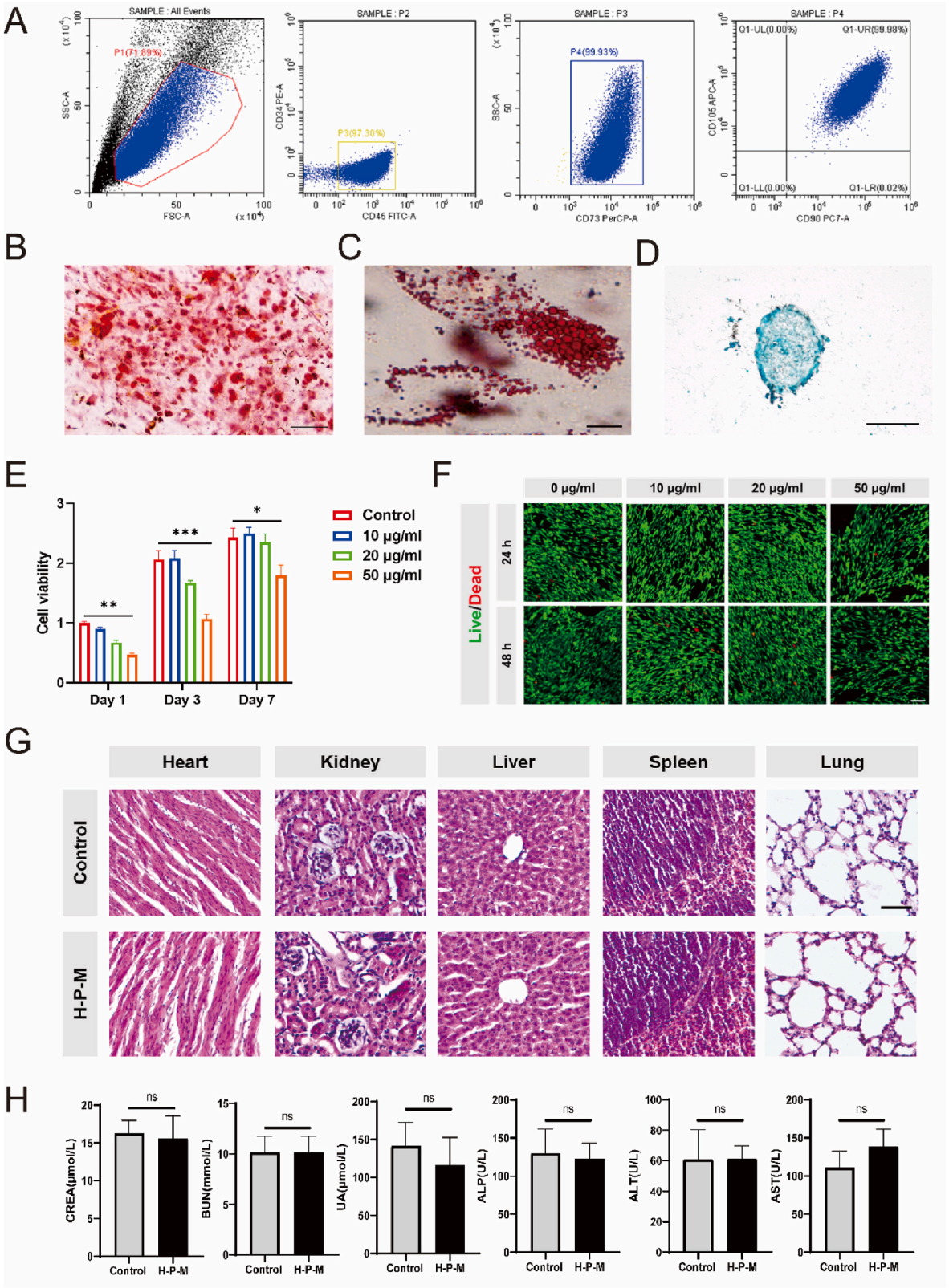

Fig. 3. The biocompatibility and biotoxicity of PDA NPs. (A) Identification of surface markers of CD34, CD45, CD73, CD90 and CD105 in hUC-MSCs through flow cytometry. (B) The capacity of osteogenic differentiation by Alizarin Red staining. Scale bar: 100 μm. (C) The capacity of adipogenic differentiation by Oil Red staining. Scale bar: 25 μm. (D) Chondrogenic differentiation capacity by Alcian Blue staining. Scale bar: 100 μm. (E) Cell viability of hUC-MSCs at 1, 3 and 7 day (s) after treatment with different concentrations of PDA NP was assessed using the CCK8 assay. (F) The Live/Dead staining of hUC-MSCs at 1 and 2 day (s) post-treatment with different concentrations of PDA NPs was performed. Live cells are indicated by calcein staining (green), and dead cells by PI staining (red). Scale bar: 100 μm. (G) HE staining images of the heart, kidney, liver, spleen and lung, 8 weeks after hydrogel implantation after in mice. Scale bar: 50 μm. (H) The indicators (CERA/BUN/UA/ALP/ALT/AST) of the liver and kidney function 8 weeks after H-P-M hydrogel implantation in mice (n = 5). Data was presented as mean ± SEM. Results were analyzed by two-way ANOVA or *t*-test. Statistical significance: *p < 0.05, **p < 0.01, ***p < 0.001.

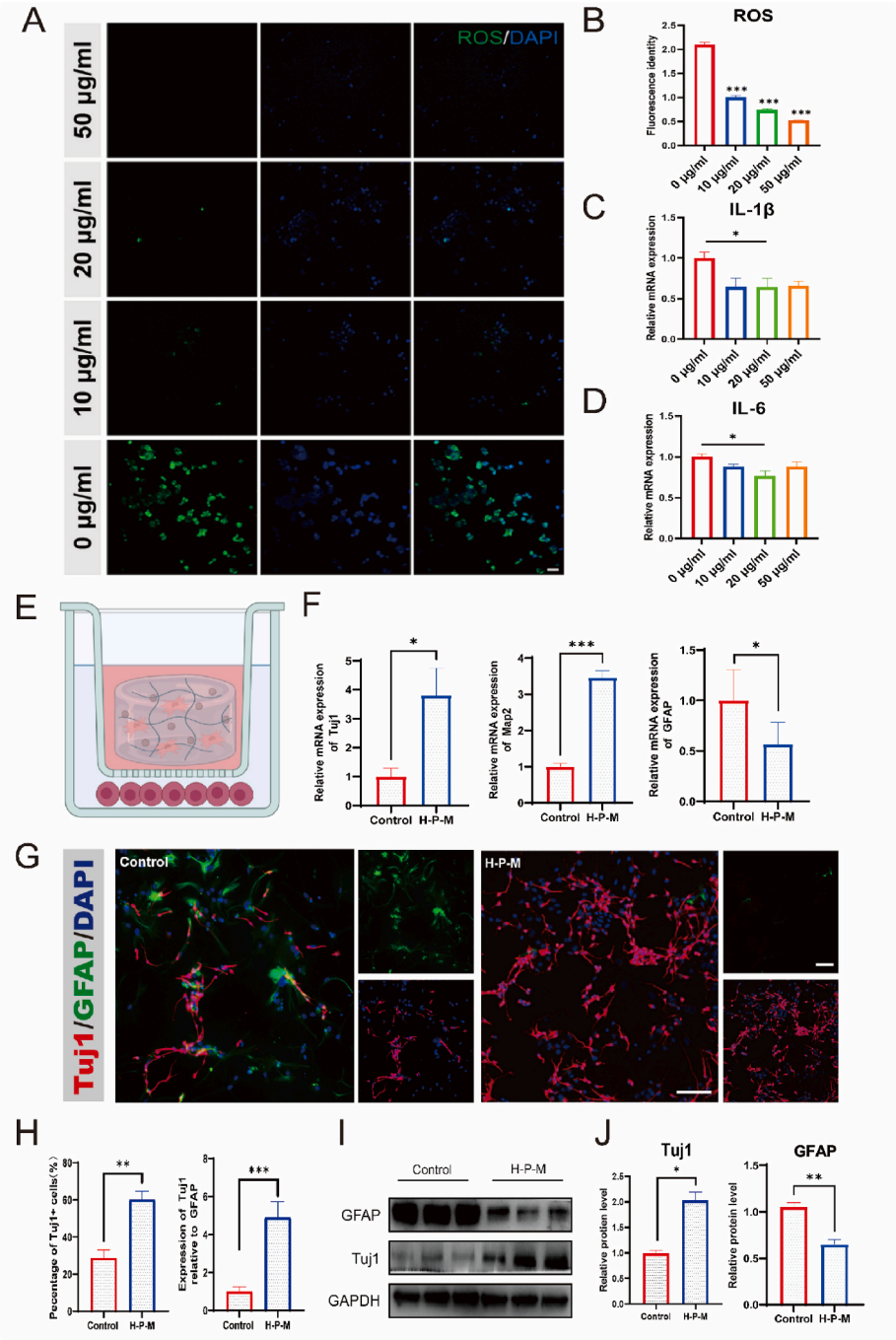

Fig. 4. Validation of H-P-M hydrogel to reduce ROS and promote NSPC neuronal differentiation *in vitro*. (A) Scavenging activity of ROS in inflammatory BV2 cells induced by LPS and treatment with PDA NPs at different concentrations (0 μg/ml, 10 μg/ml, 20 μg/ml, 50 μg/ml) of for 1 day, ROS (green), DAPI (blue). Scale bar: 50 μm. (B)The ROS level was detected by DCFH-DA in BV2 cells induced by LPS. The mRNA expression of (C) IL-1β (n = 3) and (D) IL-6 (n = 3) in BV2 cells induced by LPS. (E) Schematic diagram of co-culture of mouse NSPCs and H-P-M hydrogel. (F) The mRNA expression of Tuj1, MAP2 and GFAP after 7 days of co-culture with or w/o H-P-M hydrogel. (G) Representative images of GFAP and Tuj1 expression of NSPCs co-cultured with or w/o H-P-M hydrogel for 7 days. Scale bar: 50 μm. (H) The quantification of (G). (I and J) Western blot images showing the protein expression of GFAP and Tuj1 of NSPCs co-cultured with or w/o H-P-M hydrogel for 7 days and quantitative analysis. Data was presented as mean ± SEM. Results were analyzed by using *t*-test. Statistical significance: $^{*}p < 0.05$, $^{**}p < 0.01$, $^{***}p < 0.001$.

differentiation was evaluated in the co-cultured primary NSPCs and hydrogel-loaded hMSCs (Fig. 4E), 2.71- and 1.03- fold rise in Tuj1 mRNA and protein expression; 0.44- and 0.39- fold reduction in GFAP in the H-P-M group, indicated enhanced neuronal differentiation (Fig. 4F–J). Additionally, MAP2 mRNA expression increased by 2.46-fold (Fig. 4F). To investigate the effect of H-P-M hydrogel on oligodendrocyte differentiation, we performed IF staining for Olig2. The results showed that the average fluorescence intensity of Olig2 was significantly reduced in H-P-M group compared to control group, with the Olig2 protein expression in the H-P-M group reduced by 0.47-fold (Fig. S7–8). Together, these findings demonstrated that H-P-M hydrogel promoted neuronal differentiation of NSPCs *in vitro*.

3.4. H-P-M hydrogel induced 5-HT axon regeneration and promoted motor function recovery after SCI

To investigate the therapeutic efficacy of the H-P-M hydrogel *in vivo*, we injected the hydrogel into the lesion site immediately following surgery (Fig. 5A). HE staining showed that the lesion area was significantly reduced after 8 weeks treatment of H-P-M hydrogel (Fig. 5B), and robust 5-HT axon regeneration crossing the lesion site in the H-P-M

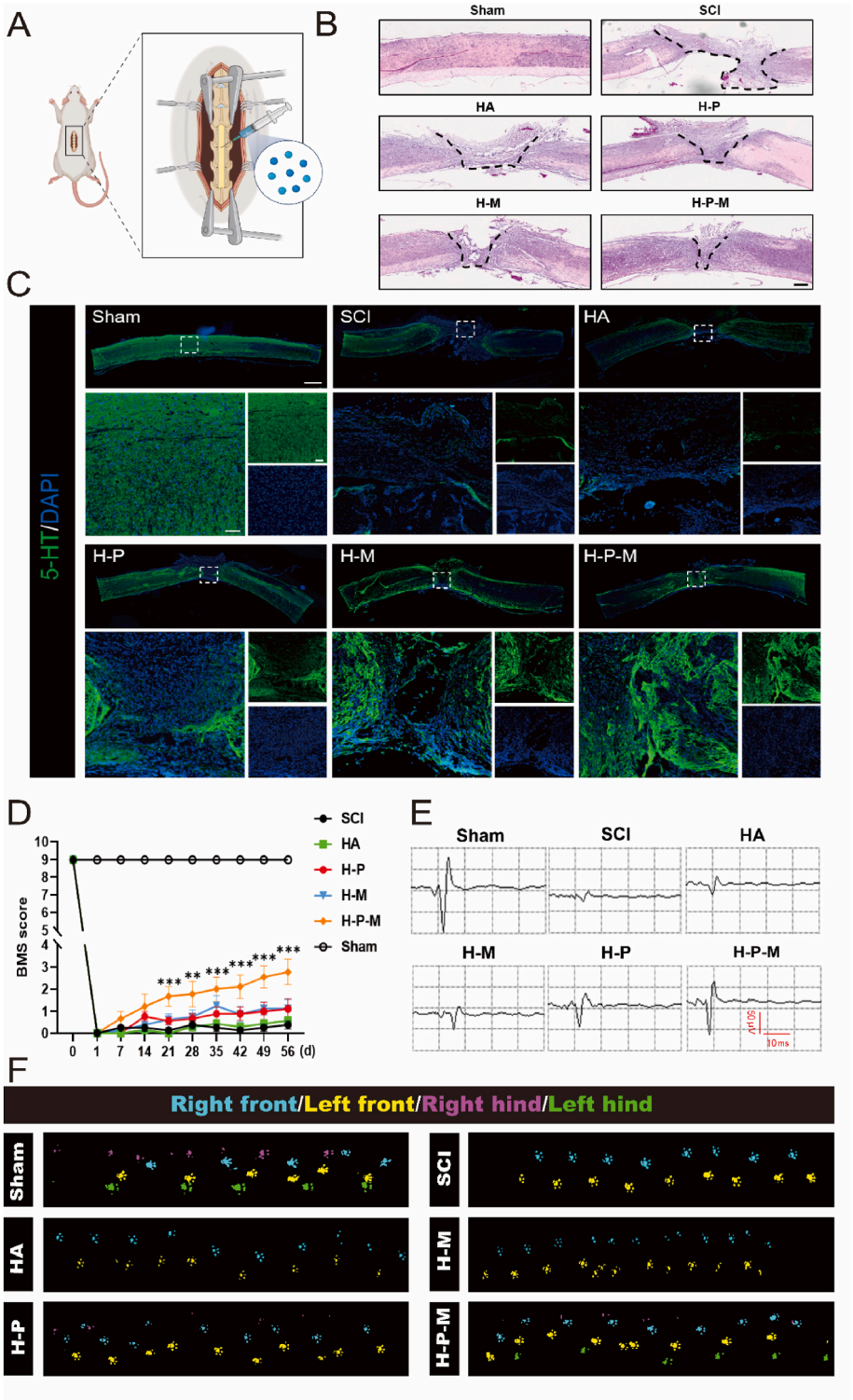

Fig. 5. H-P-M hydrogel induced 5-HT axon regeneration and promoted motor function recovery in SCI mice. (A) Schematic diagram of spinal cord transection surgery and hydrogel injection. (B) Representative images of HE-stained spinal cord section in different treatment groups. Scale bar: 500 μm. (C) Representative images of 5-HT staining of spinal cord section at 8 weeks after hydrogel injection. Scale bar (upper right): 500 μm. Scale bar (left and lower right): 50 μm. (D) The BMS scores in different treatment groups after SCI (Sham n = 8, SCI n = 8, HA n = 7, H-P n = 9, H-M n = 8, H-P-M n = 9). (E) Representative images of MEPs in different treatment groups at 8 weeks after hydrogel injection. (F) Representative images of footprints in different treatment groups at 8 weeks after hydrogel injection. Data was presented as mean ± SEM. Data were analyzed using two-way ANOVA. Statistical significance: $^{*}p < 0.05$, $^{**}p < 0.01$, $^{***}p < 0.001$.

hydrogel group, whereas such regeneration was not observed in the SCI group (Fig. 5C).

What's more important, we performed animal behavioral and electrophysiological tests to evaluate their functional recovery after treatment. Specifically, the BMS scores and gait analysis were used to assess motor function recovery in SCI mice treated with H-P-M hydrogel. At 8 week post-treatment, significant improvement in BMS score was observed in SCI mice treated with H-P-M hydrogel compared with the SCI group (Fig. 5D). Consistently, the MEP recordings confirmed a significant improvement in MEP amplitude in the H-P-M hydrogel group relative to other treatment groups (Fig. 5E, Fig. S10). Moreover, we assessed locomotion improvement by footprint recording analysis at the endpoint. Mice treated with the H-P-M hydrogel exhibited superior hindlimb movement compared with the SCI group where hindlimb movement was absent (Fig. 5F). Taken together, it demonstrated the effective enhancement of motor functional recovery following SCI with applying the H-P-M hydrogel.

3.5. *The H-P-M hydrogel exhibited the capacity to mitigate inflammatory response and facilitate the differentiation of eNSPCs into functional neurons in transected SCI mice*

To investigate the effect of H-P-M hydrogel on the recruitment and differentiation of eNSPCs, we utilized Nestin lineage tracer mice to track eNSPCs in the injured spinal cord. We found 86 % $Ki67^+$ eNSPCs labeled with tdTomato after SCI as previously reported (Fig. 6D) [18]. As illustrated in Figure 6E, a greater accumulation of eNSPCs labeled with tdTomato was observed at the injury center in the H-P-M group compared to the SCI group at 8 weeks of post-injury. In addition, we found that more eNSPCs (128.8 ± 6.83 vs 92.8 ± 8.35 cells/mm^2), especially $Ki67^+$ eNSPCs (58.6 ± 8.14 vs 19.0 ± 2.24 cells/mm^2), were recruited to peri-injury area, suggesting the great effect of H-P-M hydrogel on recruiting eNSPCs (Fig. 6F–G). Subsequently, we performed GFAP, Tuj1 and Syn1 staining to investigate the differentiation fate of eNSPCs at the injury center. The co-localization of tdTomato-positive eNSPCs with the neuronal Tuj1 and presynaptic marker Syn1 indicates the potential of recruited NSPCs to differentiate into functional neurons and integrate into the neural circuitry of the injured spinal cord (Fig. 6H–I).

The RNA-seq data showed 9160 differentially expressed genes (DEGs) in H-P-M hydrogel treated group with 5079 upregulated and 4081 downregulated genes in the mouse spinal cord tissue at 7 days of post-injury (Fig. 6A). The top 10 upregulated biological processes (BPs) include synapse organization, neurotransmitter transport and regulation of synaptic plasticity, indicating enhanced neurogenesis and synaptic activity (Fig. 6A–B). Besides, the heatmap showed that the neuronal markers (Tubb3, Map2, NeuN), motor neuron marker (Chat) and synaptic vesicle markers (Syp, Snap25) upregulated significantly (|fold change| >5 and $p < 0.05$), suggesting enhanced neurogenesis and neuronal activity (Fig. 6C). The KEGG enrichment analysis indicated that the H-P-M hydrogel primarily promoted eNSPCs neuronal differentiation through the positive regulation of the MAPK cascade signaling pathway (Fig. S11). We analyzed family proteins including ERK, JNK, p-ERK and p-JNK in the MAPK pathway, p-ERK and p-JNK were increased to 2-fold and 3.1-fold in the H-P-M hydrogel group (Fig. 6J). Importantly, GO term and GSEA showed downregulation in immune cell migration, inflammatory response and cytokine production, and in particular, inflammatory factors of iNOS, IL-1β, and IL-6 downregulated significantly (|fold change| >5 and $p < 0.05$), suggesting a reduced inflammatory response following H-P-M hydrogel injection (Fig. 7A–C). Additionally, the proinflammation factor iNOS decreased by 39 %, while anti-inflammation factor Arg1 increased by 79 % in IBA1 positive microglia, indicating an alleviated inflammatory response in the H-P-M hydrogel group (Fig. 7D–E). These findings demonstrated that H-P-M hydrogel effectively suppressed secondary inflammatory response following primary mechanical injury through the anti-inflammatory properties of PDA NPs, which contributed to axon regeneration and motor functional recovery.

4. Discussion and conclusion

During the acute (<48h) and subacute (2d-2w) stages after SCI, the lesion sites experienced microenvironmental imbalance characterized by accumulation of ROS and dysregulation of inflammation. This led to the disruption of the neuronal cell niche causing secondary neuronal loss. Consequently, the fate of endogenous neural stem cells (eNSCs) tends to differentiate into astrocytes [1,19,20]. Thus, the disruption of the lesion microenvironment and inadequate endogenous nerve regeneration represent the primary barriers to functional recovery following SCI. Over the past decade, numerous initiatives have been undertaken to facilitate nerve regeneration after SCI, including gene editing, drug intervention, stem cell transplantation and exosome delivery [16, 21–23]. However, no effective therapy established due to complex cues in the inhibitory microenvironment of SCI and deficit of endogenous nerve regeneration. Recently, studies on bioactive materials combined with neurotrophic factors present the potential to trigger neuron regeneration [4,14,16,24]. Hydrogel, in particular, is emerging as a promising candidate for SCI repair.

The intrinsic properties of the hydrogel, such as permeability, hydrophilic, biocompatibility and cell accessibility make them as suitable substrates to imitate the natural matrix [25]. Previous studies showed the combination of hydrogel and nanoparticles or bioactive peptides to address the mechanical and physiological properties of spinal cord tissue, including electrical conductivity, magnetic or mechanical properties. For example, incorporation the inorganic particles such as cerium oxide or graphene into the hydrogel provides ROS scavengers, which help improve the inflammatory microenvironment at the lesion site and create a suitable environment for the mobilization of eNSCs. In addition, the conductive hydrogel modified by metal ions, such as ferrous ion, confer magnetic or electrical conductivity to facilitate the neural circuit loop and differentiation of NSCs [26,27]. However, the poor biodegradation of inorganic particles and metal ions within hydrogel restrict its application for SCI repair. It is crucial to design a multifunctional, biodegradable, biocompatible hydrogel for improving the niche with potential therapeutic application in SCI.

In the past two decades, stem cell-based therapy has demonstrated great therapeutic potential for neurological deficits in the subacute and chronic stages of SCI, which is attributed to their ability to bridge the injury site, enhance neurite growth and facilitate myelination [28]. Among cell-based transplantation, MSCs are currently regarded as the optimal choice due to its easy accessibility, safety and low immunogenicity. In addition, our previous study along with other research demonstrated that the MSCs secretome can exert multiple unique therapeutic effects including neuroimmunomodulation, anti-inflammation, neurotrophy and angiogenesis [29–32].

However, the transplantation of MSCs still faces challenges. For example, huge tissue defects and the loss of extracellular matrix such as HA, collagen and fibronectin, lead to the failure of MSCs attachment, consequently resulting in cell death and impaired therapeutic effect [33]. In addition, severe neuroinflammation and challenges of host-graft rejection compromise to the sustained survival and proliferation of transplanted cells. Recently, the transplantation of MSCs combined with hydrogel scaffolds has emerged as a promising approach to address these challenges. Hydrogel scaffolds provide an extracellular matrix that supports MSC growth and offer crucial guidance for tissue regeneration and repair [23]. Furthermore, the functional modification of hydrogels and the incorporation of nanoparticles can create a favorable microenvironment that enhances the survival and proliferation of transplanted cells [5,34]. Therefore, we created a robust HA conjugated hydrogel combined biomolecules to trigger and sustain the efficacy of transplanted cells, resulting in a multifunctional hydrogel (H-P-M hydrogel) with adhesive property, biocompatibility, biodegradability,

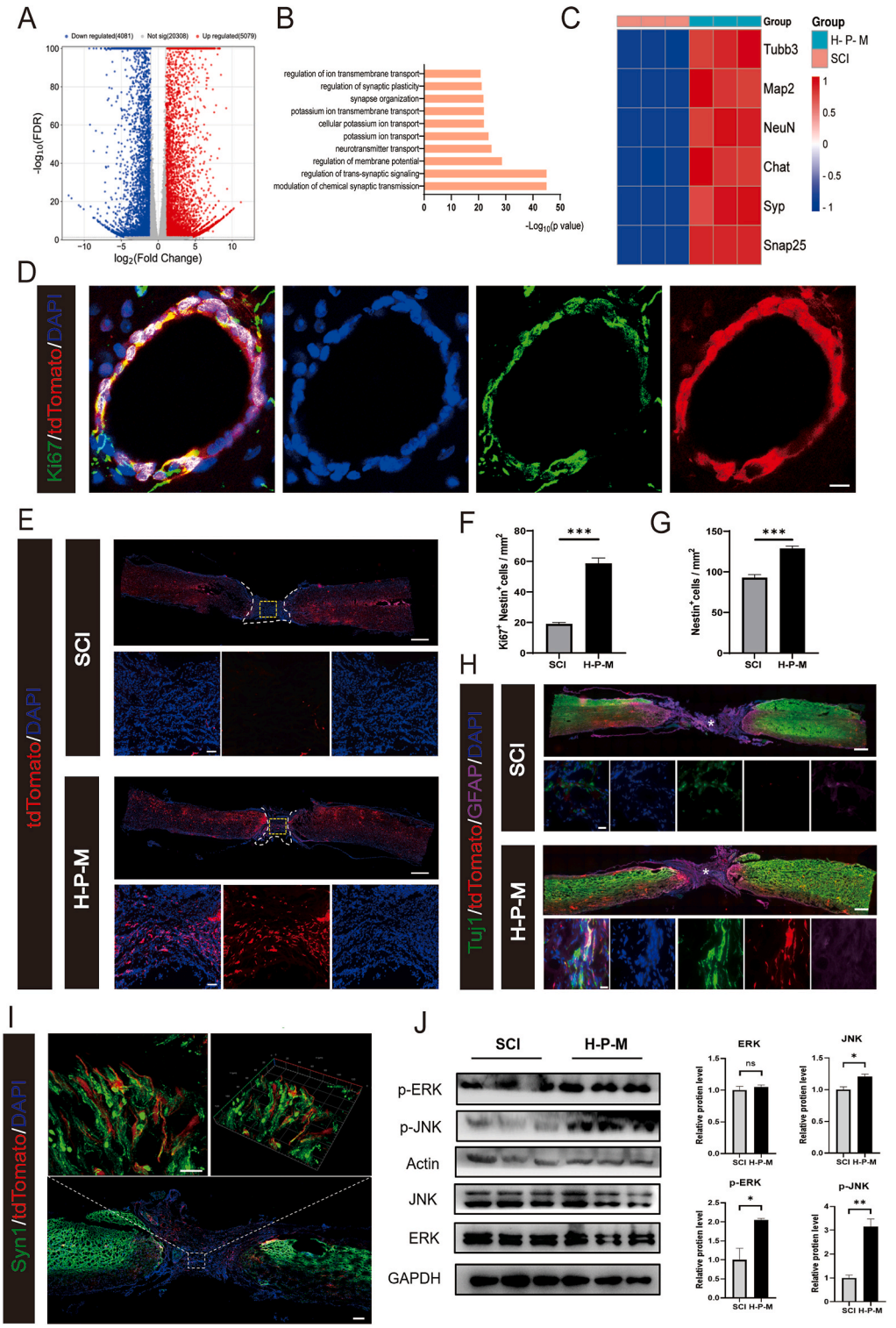

Fig. 6. H-P-M hydrogel recruited eNSPCs to the injury site and facilitated neuronal differentiation for SCI repair. (A) Results of DEGs (FDR<0.05) were displayed by a volcano plot. (B) The significantly enriched biological processes (BPs) from upregulated DEGs were presented. (C) Heat map of key genes involved in neuronal differentiation (Tubb3, Map2, NeuN and Chat) and synapse formation (Syp and Snap25). (D) Representative fluorescence images showing Ki67 staining of spinal cord section of Nestin lineage tracer mice after SCI. The eNSPCs were labeled with tdTomato (red). Nuclei were labeled with DAPI (blue) in each group. Scale bar: 20 μm. (E) Representative fluorescence images showing the recruitment of eNSPCs labeled with tdTomato (red) at the lesion site in SCI mice. Nuclei were labeled with DAPI (blue) in each group. Scale bar: 400 μm. (F–G) Quantitation of Nestin$^+$ eNSPCs and Ki67$^+$ & Nestin$^+$ proliferating eNSPCs around injury site at 8 weeks after hydrogel injection. (H)Representative fluorescence images showing Tuj1 and GFAP staining of spinal cord section at 8 weeks after hydrogel injection. The eNSPCs were labeled with tdTomato (red). Nuclei were labeled with DAPI (blue) in each group. Scale bar: 40 μm. (I) Representative fluorescence images showing Tuj1 and Syn1 staining of spinal cord section at 8 weeks after hydrogel injection. The eNSPCs were labeled with tdTomato (red). Nuclei were labeled with DAPI (blue) in each group. Scale bar: 200 μm. (J) The Western blot images and quantification showed the protein expression of JNK, ERK, p-JNK and p-ERK. Data was presented as mean ± SEM. Results were analyzed by *t*-test. Statistical significance: $^*p < 0.05$, $^{**}p < 0.01$, $^{***}p < 0.001$.

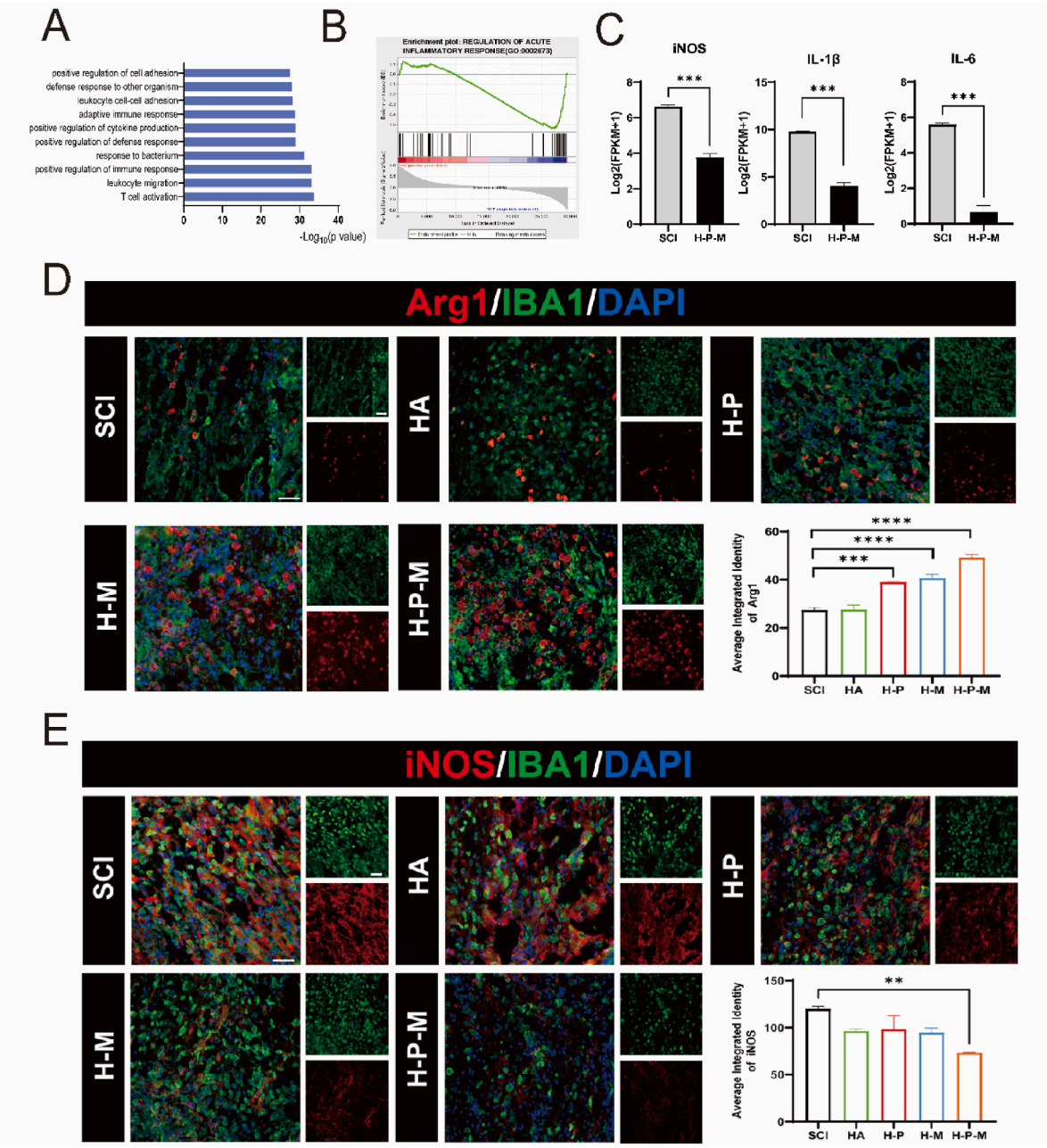

Fig. 7. H-P-M hydrogel could reduce the release of pro-inflammatory factors and inflammatory response of microglia in SCI mice. (A) The significantly enriched biological processes (BPs) from downregulated DEGs were presented. (B) GSEA of the acute inflammatory response gene set. (C) The expression of key genes involved in inflammatory response including iNOS, IL-1β and IL-6. (D) Representative fluorescence images and quantification showing Arg1 (red) and IBA1 (green) staining of spinal cord sections in each group at 1 week after hydrogel injection. Nuclei were labeled with DAPI (blue) in each group. Scale bar: 200 μm. (E) Representative fluorescence images and quantification showing iNOS (red) and IBA1 (green) staining of spinal cord sections in each group at 1 week after hydrogel injection. Nuclei were labeled with DAPI (blue) in each group. Scale bar: 200 μm. Data was presented as mean ± SEM. Results were analyzed by one-way ANOVA with the Holm-Sidak test. Statistical significance: $^{*}p < 0.05$, $^{**}p < 0.01$, $^{***}p < 0.001$.

ROS-scavenging, low-immunogenicity and anti-inflammation effects. The H-P-M hydrogel used in this study showed good biocompatibility, and the hydrogel immersed in PBS completely degraded within 14 days [5]. In addition, H-P-M hydrogel utilized PDA NPs to shield transplanted MSCs from oxidative damage, increasing their survival rate in an H_2O_2-induced peroxidative environment. Moreover, H-P-M hydrogel had a better effect on reducing pro-inflammatory factor iNOS and increasing anti-inflammatory factor Arg1 in microglia with single treatment group *in vivo* (H-M and H-P group). PDA NPs have been reported to reduce oxidative and inflammatory damage in multiple disease models. They can reduce lipid peroxidation induced by ROS. On the other hand, PDA NPs are capable of adsorbing excessive cytokines due to their adhesive property [35,36]. Unlike previous studies, our research demonstrates the protective effect of our approach on MSCs in a peroxidative environment and its synergistic impact on spinal cord injury repair.

The eNSPCs are nervous tissue-specific adult stem cells with the capacity to differentiate into neurons and glial cells, and they could proliferate rapidly and migrate to the lesion site while activating in SCI [37]. In this study, H-P-M hydrogel established a permissive niche for the recruitment of eNSPCs and neuronal differentiation through favorable extracellular matrix and exogenous MSCs transplantation. Our data

showed that the number of labeled eNSPCs in both the injury center and peri-injury area was significantly increased in the H-P-M group, demonstrating the capacity of the multifunctional hydrogel to recruit eNSPCs. Furthermore, the enhanced neuronal differentiation of eNSPCs at the injury center, establishing synaptic connections with the survival of neurons and integrating into the local neural circuit. Given that the endogenous neurogenesis after SCI contributes to motor functional recovery, we performed behavioral assessments at 8 weeks after SCI. As expected, significant improvement in BMS scores and larger MEP amplitudes of hindlimbs was seen in the H-M-P group compared with the SCI naïve treatment at 8 weeks of post-treatment. Moreover, superior hindlimb movement in mice treated with H-P-M hydrogel was observed from our gait recording analysis. The above-mentioned improvement in motor function was also confirmed by stronger 5-HT axon regeneration in the H-P-M group.

Further transcriptome analyses indicated a predominant association with enhanced neurogenesis and inhibited immune response. Previous studies have reported that MAPK signaling pathway activation, particularly the upregulation of p-ERK and p-JNK, is involved in the neuronal differentiation of eNSPCs, which is consistent with our result of KEGG enrichment analysis. Additionally, we found that the top 10 downregulated BPs included the T cell activation and adaptive immune response, suggesting a favorable niche with the low immune response after the treatment of H-P-M hydrogel, consequently promoting the survival of transplanted cells and eNSPCs.

Our research takes advantage of the synergistic interplay of multiple functions to engineer a favorable niche facilitating the neuronal differentiation of eNSPCs, thereby contributing to rebuilding the neural circuits in the injured spinal cord. The uncontrolled migration of MSCs may be a weakness in our strategy. In the future, we will focus on enhancing the targeting capabilities of MSCs and enhancing their retention at the injury site to achieve the optimal therapeutic outcomes.

Ethics approval and consent to participate

All the animal experiments were approved by the Ethics Committee of Qilu Hospital, Shandong University (SYKX:20230003). All the authors compliance with all relevant ethical regulations.

CRediT authorship contribution statement

Yanbing Kao: Writing – original draft, Validation, Methodology, Investigation, Data curation. **Wei Song:** Writing – original draft, Validation, Methodology, Investigation, Formal analysis, Data curation. **Renjie Zhang:** Writing – original draft, Validation, Methodology, Investigation, Data curation. **Guangjin Gu:** Writing – original draft, Validation, Methodology, Investigation, Data curation. **Heping Qiu:** Software, Resources. **Wenyuan Shen:** Writing – original draft, Validation, Methodology, Investigation, Data curation. **Hanming Zhu:** Writing – original draft, Validation, Methodology, Investigation, Data curation. **Yanchun Liu:** Writing – original draft, Validation, Methodology, Investigation, Conceptualization. **Yu Yang:** Writing – original draft, Validation, Methodology, Investigation, Data curation. **Haoyun Liu:** Writing – original draft, Validation, Methodology, Investigation, Data curation. **Zhihao Zhang:** Writing – original draft, Validation, Methodology, Investigation, Data curation. **Xiaohong Kong:** Writing – review & editing, Resources, Project administration, Funding acquisition, Conceptualization. **Shiqing Feng:** Writing – review & editing, Resources, Project administration, Funding acquisition, Conceptualization.

Declaration of competing interest

The authors declare that they have no known competing financial interests or personal relationships that could have appeared to influence the work reported in this paper.

Acknowledgments

This work was supported by the National Natural Science Foundation of China (82172417), the National Key Research and Development Project of Stem Cell and Transformation Research (2019YFA0112100), China and Talent project of Shandong University (22480082063100), China. We thank the Translational Medicine Core Facility of Shandong University for the consultation and instrument availability that supported this work.

Appendix A. Supplementary data

Supplementary data to this article can be found online at https://doi.org/10.1016/j.bioactmat.2024.09.027.

References

[1] B. Fan, et al., Progression in translational research on spinal cord injury based on microenvironment imbalance, Bone Res 10 (2022) 35, https://doi.org/10.1038/s41413-022-00199-9.
[2] M.V. Sofroniew, Dissecting spinal cord regeneration, Nature 557 (2018) 343–350, https://doi.org/10.1038/s41586-018-0068-4.
[3] B. Fan, et al., Microenvironment imbalance of spinal cord injury, Cell Transplant. 27 (2018) 853–866, https://doi.org/10.1177/0963689718755778.
[4] B. Zhu, et al., Schwann cell-derived exosomes and methylprednisolone composite patch for spinal cord injury repair, ACS Nano 17 (2023) 22928–22943, https://doi.org/10.1021/acsnano.3c08046.
[5] L. Li, et al., A MnO2 nanoparticle-dotted hydrogel promotes spinal cord repair via regulating reactive oxygen species microenvironment and synergizing with mesenchymal stem cells, ACS Nano 13 (2019) 14283–14293, https://doi.org/10.1021/acsnano.9b07598.
[6] J.A. Burdick, G.D. Prestwich, Hyaluronic acid hydrogels for biomedical applications, Adv. Mater. 23 (2011), https://doi.org/10.1002/adma.201003963.
[7] L.M. Li, et al., Peptide-tethered hydrogel scaffold promotes recovery from spinal cord transection via synergism with mesenchymal stem cells, ACS Appl. Mater. Interfaces 9 (2017) 3330–3342, https://doi.org/10.1021/acsami.6b12829.
[8] T. Führmann, et al., Click-crosslinked injectable hyaluronic acid hydrogel is safe and biocompatible in the intrathecal space for ultimate use in regenerative strategies of the injured spinal cord, Methods 84 (2015) 60–69, https://doi.org/10.1016/j.ymeth.2015.03.023.
[9] M. d'Ischia, et al., Polydopamine and eumelanin: from structure–property relationships to a unified tailoring strategy, Acc. Chem. Res. 47 (2014) 3541–3550, https://doi.org/10.1021/ar500273y.
[10] H. Zhao, et al., Polydopamine nanoparticles for the treatment of acute inflammation-induced injury, Nanoscale 10 (2018) 6981–6991, https://doi.org/10.1039/c8nr00838h.
[11] H. Lee, et al., Mussel-inspired surface chemistry for multifunctional coatings, Science 318 (2007) 426–430, https://doi.org/10.1126/science.1147241.
[12] X. Bao, et al., Polydopamine nanoparticles as efficient scavengers for reactive oxygen species in periodontal disease, ACS Nano 12 (2018) 8882–8892, https://doi.org/10.1021/acsnano.8b04022.
[13] Y. Kao, et al., CREB1 facilitates GABAergic neural differentiation of human mesenchymal stem cells through BRN2 for pain alleviation and locomotion recovery after spinal cord injury, Cells 13 (2023), https://doi.org/10.3390/cells13010067.
[14] M. Hao, et al., HAp thermosensitive nanohydrogel cavities act as brood pouches to incubate and control-release NSCs for rapid spinal cord injury therapy, Adv. Funct. Mater. 32 (2022), https://doi.org/10.1002/adfm.202203492.
[15] Z. Luo, et al., Human bone marrow mesenchymal stem cell-derived extracellular vesicles inhibit shoulder stiffness via let-7a/Tgfbr1 axis, Bioact. Mater. 17 (2022) 344–359, https://doi.org/10.1016/j.bioactmat.2022.01.016.
[16] N. Ran, et al., Autologous exosome facilitates load and target delivery of bioactive peptides to repair spinal cord injury, Bioact. Mater. 25 (2023) 766–782, https://doi.org/10.1016/j.bioactmat.2022.07.002.
[17] B. Zhang, et al., Injectable, electroconductive, free radical scavenging silk fibroin/black phosphorus/glycyrrhizic acid nanocomposite hydrogel for enhancing spinal cord repair, 13, https://doi.org/10.1002/adhm.202304300, 2024.
[18] X. Xue, et al., Lineage tracing reveals the origin of Nestin-positive cells are heterogeneous and rarely from ependymal cells after spinal cord injury, Sci. China Life Sci. 65 (2022) 757–769, https://doi.org/10.1007/s11427-020-1901-4.
[19] E.A.B. Gilbert, et al., Regulating endogenous neural stem cell activation to promote spinal cord injury repair, Cells 11 (2022), https://doi.org/10.3390/cells11050846.
[20] Z. Li, et al., A reactive oxygen species-responsive hydrogel encapsulated with bone marrow derived stem cells promotes repair and regeneration of spinal cord injury, Bioact. Mater. 19 (2023) 550–568, https://doi.org/10.1016/j.bioactmat.2022.04.029.
[21] K. Liu, et al., PTEN deletion enhances the regenerative ability of adult corticospinal neurons, Nat. Neurosci. 13 (2010) 1075–1081, https://doi.org/10.1038/nn.2603.
[22] H. Ma, et al., Tofacitinib promotes functional recovery after spinal cord injury by regulating microglial polarization via JAK/STAT signaling pathway, Int. J. Biol. Sci. 19 (2023) 4865–4882, https://doi.org/10.7150/ijbs.84564.

[23] P. Assinck, et al., Cell transplantation therapy for spinal cord injury, Nat. Neurosci. 20 (2017) 637–647, https://doi.org/10.1038/nn.4541.
[24] M. Hao, et al., Multifunctional hydroxyapatite nanobelt haystacks integrated neural stem cell spheroid for rapid spinal cord injury repair, Adv. Funct. Mater. 33 (2023), https://doi.org/10.1002/adfm.202214869.
[25] Y. Wang, et al., Multimodal therapy strategies based on hydrogels for the repair of spinal cord injury, Mil Med Res 9 (2022) 16, https://doi.org/10.1186/s40779-022-00376-1.
[26] Y. Niu, et al., Recent advances of magnetic chitosan hydrogel: preparation, properties and applications, Int. J. Biol. Macromol. 247 (2023) 125722, https://doi.org/10.1016/j.ijbiomac.2023.125722.
[27] B. Sung, et al., Magnetic microgels and nanogels: physical mechanisms and biomedical applications, Bioeng Transl Med 6 (2021) e10190, https://doi.org/10.1002/btm2.10190.
[28] C.M. Zipser, et al., Cell-based and stem-cell-based treatments for spinal cord injury: evidence from clinical trials, Lancet Neurol. 21 (2022) 659–670, https://doi.org/10.1016/s1474-4422(21)00464-6.
[29] F. Cofano, et al., Mesenchymal stem cells for spinal cord injury: current options, limitations, and future of cell therapy, Int. J. Mol. Sci. 20 (2019), https://doi.org/10.3390/ijms20112698.
[30] J. Qu, H. Zhang, Roles of mesenchymal stem cells in spinal cord injury, Stem Cell. Int. 2017 (2017) 1–12, https://doi.org/10.1155/2017/5251313.
[31] Y. Yang, et al., Subarachnoid transplantation of human umbilical cord mesenchymal stem cell in rodent model with subacute incomplete spinal cord injury: preclinical safety and efficacy study, Exp. Cell Res. 395 (2020), https://doi.org/10.1016/j.yexcr.2020.112184.
[32] H. Tang, et al., Human umbilical cord mesenchymal stem cell-derived exosomes loaded into a composite conduit promote functional recovery after peripheral nerve injury in rats, Neural Regen Res 19 (2024) 900–907, https://doi.org/10.4103/1673-5374.380911.
[33] G. Li, et al., An NT-3-releasing bioscaffold supports the formation of TrkC-modified neural stem cell-derived neural network tissue with efficacy in repairing spinal cord injury, Bioact. Mater. 6 (2021) 3766–3781, https://doi.org/10.1016/j.bioactmat.2021.03.036.
[34] X. Wang, et al., Anti-stress and anti-ROS effects of MnOx-functionalized thermosensitive nanohydrogel protect BMSCs for intervertebral disc degeneration repair, Adv. Healthcare Mater. (2024), https://doi.org/10.1002/adhm.202400343.
[35] G. Jensen, et al., Hyaluronic acid biomaterials for central nervous system regenerative medicine, Cells 9 (2020), https://doi.org/10.3390/cells9092113.
[36] Y. Wang, et al., Combination of hyaluronic acid hydrogel scaffold and PLGA microspheres for supporting survival of neural stem cells, Pharm. Res. (N. Y.) 28 (2011) 1406–1414, https://doi.org/10.1007/s11095-011-0452-3.
[37] X. Hu, et al., Spinal cord injury: molecular mechanisms and therapeutic interventions, Signal Transduct. Targeted Ther. 8 (2023), https://doi.org/10.1038/s41392-023-01477-6.